processes

MDPI

Article

Temperature–Electrokinetic Co-Driven Perfluorooctane Sulfonic Acid (PFOS) Adsorption on Geo-Adsorbents

Yuzhou Yin [1,†], Yongping Shan [2,†], Dong Ma [2], Liuqing Yang [2], Mingxiu Zhan [3], Ping Liu [2], Benzhen Lou [2], Bo Zhang [2], Wentao Jiao [2] and Lichu Yin [1,*]

1 College of Resources, Hunan Agricultural University, Changsha 410128, China
2 Research Center for Eco-Environmental Sciences, Chinese Academy of Sciences, Beijing 100085, China
3 College of Metrology and Measurement Engineering, China Jiliang University, Hangzhou 310018, China
* Correspondence: lcyin@hunau.edu.cn; Tel.: +86-135-1747-9381
† These authors contributed equally to this work.

Abstract: Per- and polyfluoroalkyl substances (PFAS) have concerned the public due to their worldwide distribution and the threat they pose to drinking water safety and human health. Temperature and DC field-induced electroosmotic flow (EOF) are powerful tools to regulate organic contaminant adsorption and control PFOS (as a typical PFAS) transport in porous media. However, the co-driven mechanisms of temperature–electrokinetic transport of contaminants are still unclear. Here, we investigated the synergistic mechanisms of temperature–electrokinetic co-driven PFOS adsorption on zeolite and activated carbon as model geo-adsorbents. We found that DC fields increased PFOS adsorption on activated carbon by up to 19.8%, while they decreased PFOS adsorption on zeolite by up to 21.4%. Increasing the temperature decreased the adsorption of PFOS by activated carbon and zeolite. The temperature and electrokinetic synergistically drive EOF velocity to control PFOS adsorption. Synergistic mechanisms of temperature–electrokinetic regulated kinetic and temperature-regulated thermodynamic (the Gibbs free energy change ΔG) and kinetic (liquid viscosity) under various temperatures and DC field situations were analyzed with models. A kinetic approach interlinking viscosity, EOF velocity, and the kinetic adsorption constants was established to interpret the synergistic mechanisms which can be further adopted to estimate temperature–electrokinetic induced PFOS adsorption benefits to mineral and carbonaceous adsorbents. We concluded that such kinetic regulation may provide support for controlling the transmission of PFOS.

Keywords: PFOS; temperature; electrokinetic; electroosmotic flow; adsorption kinetics; adsorption thermodynamics

Citation: Yin, Y.; Shan, Y.; Ma, D.; Yang, L.; Zhan, M.; Liu, P.; Lou, B.; Zhang, B.; Jiao, W.; Yin, L. Temperature–Electrokinetic Co-Driven Perfluorooctane Sulfonic Acid (PFOS) Adsorption on Geo-Adsorbents. *Processes* **2023**, *11*, 1856. https://doi.org/10.3390/pr11061856

Academic Editor: Andrea Melchior

Received: 27 March 2023
Revised: 31 May 2023
Accepted: 14 June 2023
Published: 20 June 2023

1. Introduction

In the past decades of industrial production and consumer usage, per- and polyfluoroalkyl substances (PFAS) have grown to be one of the most important of environmental contaminations, garnering public, scientific, and regulatory concerns [1]. Related studies have shown associations between exposure to specific PFAS and various health effects, including altered thyroid and immune system dysfunction [2,3], lipid dysregulations [4,5], and kidney diseases [6,7]. Perfluorooctane sulfonic acid (PFOS) is one of the most frequently detected PFAS [8,9] and is extremely resistant to biodegradation [10–13] due to the extreme stability of the C-F bond [14,15]. Therefore, removing PFOS from environmental matrices becomes an important issue. Adsorption is an effective method for controlling the PFOS concentration in soil and water, particularly at high concentration point source pollution sites [16–19], where rapid adsorption kinetics and preventing the formation of more difficult-to-manage short-chain byproducts are crucial [20,21].

Prior adsorption investigations were performed with a view to creating novel adsorbent materials [22,23] and external controlling techniques. Mechanisms of external

controlling techniques such as temperature [24,25] and DC field induced electrokinetic [26] have been applied to adsorption processes. These techniques may elevate the performance of commercial adsorbents such as activated carbon.

Temperature controls adsorption kinetics by altering the liquid viscosity [27] and adsorption thermodynamics by altering the interaction energy [28]. Electroosmotic flow (EOF), as a pore fluid flow induced by electrokinetic-driven ion movement on the solid surface [29,30], is a powerful tool to control the adsorption kinetics by transporting chemical molecules through the pores of adsorbent particles [26]. The adsorption/desorption of chemicals from geo-adsorbents can be speeded up using EOF, while the adsorption capacity will vary with temperature [31]. In the application of electrokinetic regulated adsorption processes, temperature effects exist at the same time. However, the synergistic mechanisms are still unclear. Consequently, the aim of our investigations is to elucidate the temperature–electrokinetic synergistic mechanisms governing the PFOS adsorption processes.

In this study, the temperature–electrokinetic adsorption of PFOS on porous column media packed with two common geo-adsorbents, activated carbon (carbonaceous adsorbent) and zeolite (mineral adsorbent), were investigated. Temperature and electrokinetic adsorption kinetics were discussed using a pseudo-second-order kinetic model. Moreover, temperature adsorption thermodynamics were calculated using Freundlich isotherms at varying temperatures. An approach connecting EOF, liquid viscosity, and the resulting adsorption kinetic constants was used to anticipate temperature–electrokinetically controlled adsorption. The findings of this research contributed to a knowledge of the individual and co-driving processes of temperature and electrokinetically controlled adsorption, enabling quantitative control of the transport and destiny of PFOS on geo-adsorbents.

2. Materials and Methods

2.1. Chemicals

The solutions used in this study were prepared using ultra-pure water with resistivity larger than 18.2 MΩ·cm (Millipore, Burlington, MA, USA). PFOS (95%) was purchased from J&K Scientific (Beijing, China). Potassium dihydrogen phosphate (99.5%) and dipotassium hydrogen phosphate (AR 98%) were acquired from Macklin (Shanghai, China).

Zeolite (Permutit, Si/Al (2.5), CAS:1318-02-1) and activated carbon were acquired from Macklin (Shanghai, China).

2.2. Characterization of Activated Carbon and Zeolite

A six-station specific surface area analyzer was used to determine the specific surface area and pore size of activated carbon and zeolites (ASAP 2460, Micromeritics, Norcross, GA, USA) [32]. The zeta potential of the two adsorbents was determined using a zeta-potential analyzer (ZS90, Malvern Instruments UK Ltd., Malvern, UK) with disposal folded capillary cells [33].

2.3. Determination of PFOS Concentration

PFOS was quantified using LC-MS/MS (1290-6460, Agilent, Santa Clara, CA, USA) on an Agilent ZOBRAX RR Eclipse Plus C18 column, with calibration curves established using PFOS standards (J&K Scientific, Beijing, China). The LC-MS/MS measurements were conducted with the following parameters: column temperature 30 °C, injection volume 10 μL, and flow rate 0.4 mL min^{-1}. Mobile phases of methanol and 10 mmol L^{-1} ammonium acetate were mixed with a gradient procedure (Table 1). Multiple reaction monitoring (MRM) scanning (precursor ion: 498.85 and product ion: 79.97) with electron spray ionization (ESI (−)) mode was adopted to quantitatively determine PFOS. A total of 10 calibration standards ranging from 0.01 to 10 mg L^{-1} were determined at the start of each measurement batch, and 3 calibration curves were established using standards 0.01–0.1 mg L^{-1}, 0.1–1 mg L^{-1}, and 1–10 mg L^{-1}, to satisfy the quantification of various PFOS concentration ranges (Figure 1) [34], with batch sample number ≤ 50 and $R^2 \geq 0.999$ to ensure data quality.

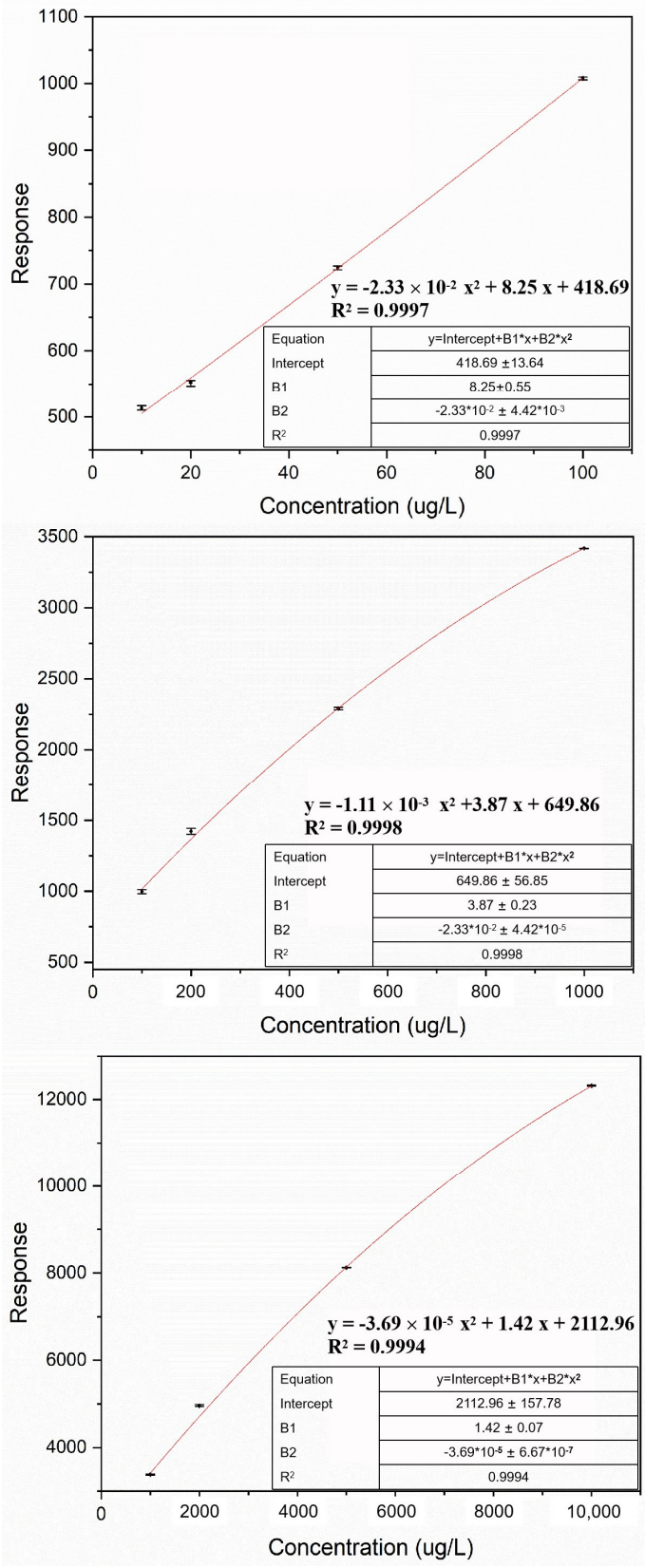

Figure 1. Calibration curves of LC-MS/MS with PFOS concentration ranges 0.01 to 0.1 mg L^{-1}, 0.1 to 1.0 mg L^{-1}, and 1.0 to 10.0 mg L^{-1}, separately.

Table 1. The gradient of the mixture of mobile phase liquids.

Time (min)	Methanol (%)	10 mM Ammonium Acetate (%)
0.00	30	70
0.30	30	70
0.40	90	10
2.50	90	10
2.60	30	70
6.00	30	70

2.4. Kinetics of PFOS Adsorption

2.4.1. Adsorption Kinetic Experiments

The electrokinetic porous media adsorption column reactor was designed according to Figure 2, the percolation column was design as described in our previous research [31]. The column reactor was filled with 100 mmol L^{-1} potassium phosphate buffer (PB: i.e., K_2HPO_4 and KH_2PO_4, pH = 7), and wet-packed with 6 g zeolite or 2.4 g activated carbon to form porous media before each experiment. The particle size of the zeolite and activated carbon used in column experiments was 0.25 to 0.43 mm. To ensure that the pH was not affected throughout the experiment, PB was used for the preparation of the stock solution and the pH was tested before and after the test with an error of no more than 0.2. Two disc-shaped Ti/Ir electrodes at the top (cathode) and bottom (anode) of the column were connected to a power pack to produce electric field strengths of 1 V cm^{-1}, 2 V cm^{-1}, and 3 V cm^{-1}, resulting in stable direct currents of 0.009~0.012 A, 0.028~0.036 A, and 0.047~0.054 A. The peristaltic pump drove the PFOS solution through the porous media downstream at a velocity of 19.6 mL h^{-1}. The liquid is kept in and out of water balance by gravity and the EOF does not change the overall flow rate. Additionally, the columns and PFOS storage solution were maintained at constant temperature in a water bath with a thermostatic circulation pump (DLSB-5L/10, Yuhua, Zhengzhou, China) to control static temperatures under 10, 20, 30, 40, and 50 °C with deviations ≤2 °C. The peristaltic pump ran 100 mmol L^{-1} PB at 19.6 mL h^{-1} for one hour before experiments allowing the system to equilibrate. Then, 10 mg L^{-1} (for zeolite) or 100 mg L^{-1} (for activated carbon) PFOS solution was pumped through the column. An amount of 1.0 mL liquid of the inlet and outlet solution was sampled at certain intervals for 48 h. These samples were centrifuged at 5000× *g* rpm (DL-5-B, Anting, Shanghai, China) and measured with LC-MS/MS. Triplicate experiments were conducted for each experimental condition.

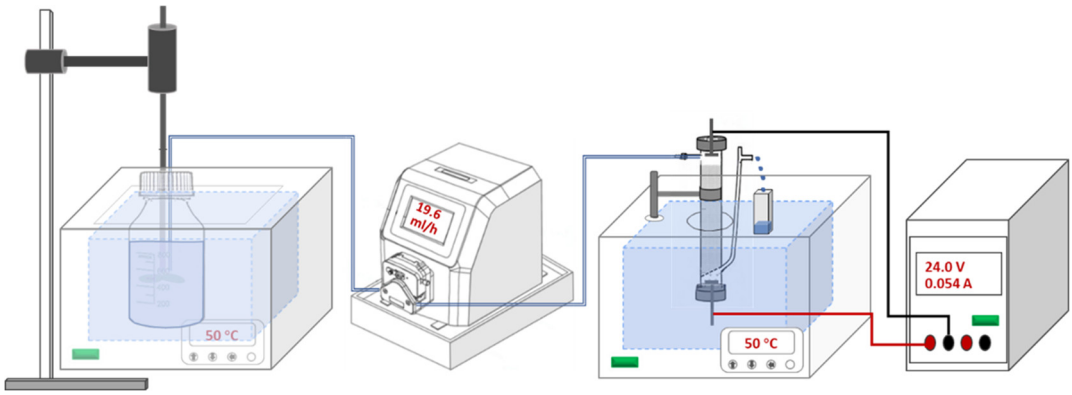

Figure 2. Schematic view of the electrokinetic setup used for adsorption experiments. PFOS solution in PB buffer in a 1000 mL reagent bottle was kept thermostatic in a water bath and driven through a column from top to bottom. The column was kept thermostatic in a water bath and electric fields applied with a DC power generator [31].

2.4.2. Adsorption Kinetic Models

Pseudo-first-order and pseudo-second-order kinetic models were adopted to investigate the adsorption kinetics. The equations were described as follows:

Pseudo-first-order (PFO) equation:

The PFO equation [35] can be expressed using

$$\ln(q_e - q_t) = -k_1 t + \ln q_e \quad (1)$$

where q_e and q_t are the PFOS concentrations in the adsorbent at equilibrium and at time t (h), respectively, while k_1 is the PFO kinetic constant.

Pseudo-second-order [36] equation:

Expression for the linear form with a plot of t/q_t versus. t [37]:

$$\frac{t}{q_t} = \left(\frac{1}{q_e}\right) t + \frac{1}{k_2 q_e^2} \quad (2)$$

where k_2 (g mg^{-1} min $^{-1}$) is the PSO kinetic constant.

2.5. Thermodynamics of PFOS Adsorption

2.5.1. Adsorption Isotherm Experiments

Isotherm batch experiments were carried out in 100 mmol L^{-1} PB in sealed 15 mL polypropylene centrifugal tubes with adsorbent-to-liquid ratios of 1:1000 (g mL^{-1}) for zeolite and 1:20,000 (g mL^{-1}) for activated carbon. The 8 initial PFOS concentrations ranged from 1.0 to 8.0 mg L^{-1} for zeolite and 10 to 80 mg L^{-1} for activated carbon, separately. The adsorbents and liquids were allowed to equilibrate in a horizontal shaker (HNY-200B, Ounuo, China) at 150 rpm for 7 days at controlled static temperatures of 10 °C, 20 °C, 30 °C, 40 °C, and 50 °C, with deviations $\leq$2 °C. To shorten the time required for adsorption equilibrium, activated carbon and zeolite were ground into fine particles (average diameter 74 $\pm$ 4 µm). After 7 days, the supernatant was derived using centrifugation at 5000$\times$ g rpm to allow PFOS concentration measurements using LC-MS/MS. All experiments were conducted in triplicate.

2.5.2. Adsorption Isotherms

Adsorption isotherms were analyzed with the Langmuir equation and Freundlich equation [38].

The non-linear form of the Langmuir equation [39] is described in Equation (3).

$$q_e = \frac{Q_{max} K_L C_e}{1 + K_L C_e} \quad (3)$$

The linear form of the Langmuir equation is defined in Equation (4).

$$\frac{1}{q_e} = \frac{1}{Q_{max} K_L C_e} + \frac{1}{Q_{max}} \quad (4)$$

where q_e (mg g^{-1}) is PFOS concentration in the adsorbent at equilibrium, Q_{max} (mg g^{-1}) is the maximum saturated monolayer adsorption capacity of the adsorbent, C_e (mg L^{-1}) is PFOS concentration in liquid at equilibrium, and K_L (L mg^{-1}) is a constant related to the affinity between the adsorbent and adsorbate.

Freundlich equation can be described by Equation (5) [37]

$$\log q_e = \log K_F + n \log C_e \quad (5)$$

where n is the Freundlich exponent as a measure of adsorption linearity, and K_F is the Freundlich isotherm constant (mg kg^{-1}) (L mg^{-1})^n.

2.5.3. Adsorption Thermodynamic Model

Thermodynamic parameters were calculated based on the isotherms measured from 10 to 50 °C. The relationship between ΔG, ΔH and ΔS was described by equation: [40]

$$\Delta G = \Delta H - T\Delta S \quad (6)$$

where the ΔH (kJ mol^{-1}) is the enthalpy change, T is the temperature in Kelvin, and the ΔS (kJ mol^{-1} K^{-1}) is the entropy change. while ΔG can be calculated according to the equation:

$$\Delta G = -RT \ln K_c \quad (7)$$

K_c is the equilibrium constant (being dimensionless), and based on the Freundlich isotherm parameter K_F and the aqueous density, K_c can be calculated by

$$K_c = \frac{K_F \rho}{1000} \left(\frac{10^6}{\rho} \right)^{(1-n)} \quad (8)$$

ΔH can be estimated using the van't Hoff equation by substituting Equation (8) for Equation (6)

$$\ln K_c = -\frac{\Delta H}{R} \times \frac{1}{T} + \frac{\Delta S}{R} \quad (9)$$

where R is the gas constant (8.314×10^{-3} kJ mol^{-1} K^{-1}). The values of ΔH can be estimated using the slope and intercept of a plot of ln K_c vs. T^{-1}, and ΔH and ΔG can help to calculate ΔS (Equation (6)).

2.6. Quantification of the EOF Velocities

The EOF velocity ($V_{EOF,r}$) in an intra-particle [41] pore of radius r can be calculated using $V_{EOF,max}$ and a function of κr [42] (i.e., $f(kr)$) as detailed by Equations (10)–(12):

$$V_{EOF,r} = V_{EOF,max} * f(kr) \quad (10)$$

$$V_{EOF,max} = -\frac{\varepsilon_r \varepsilon_0 X \xi}{\eta} \quad (11)$$

$$f(kr) = \left(1 - \frac{2I_1(kr)}{krI_0(kr)} \right) \quad (12)$$

where ε_r is the dielectric constant of water (78.5), ε_0 (8.85×10^{-12} F m^{-1}) is the vacuum permittivity, η is the liquid viscosity (Pa·s), ξ is the zeta potential (V) of the solid surface, X is the electric field strength (V m^{-1}), I_0 and I_1 are the zero and first-order modified Bessel functions, and κ^{-1} is the thickness of the electrical double layer (nm) calculated using the Guoy–Chapman theory.

$$k^{-1} = \left(3.29 z C_1^{\frac{1}{2}} \right)^{-1} \quad (13)$$

where C_1 and z are the molar bulk concentration and the charge number of the electrolytes, respectively [43].

3. Results

3.1. Temperature–Electrokinetic Regulated Adsorption Breakthrough Curves

Physicochemical properties of the adsorbents were investigated in the first instance, including specific surface area, average pore size, and zeta potential (Table 2). The activated carbon has a larger specific surface area of 144.4 m^2 g^{-1}, comparing to 2.9 m^2 g^{-1} for zeolite, while the two absorbents have a similar average intra-particle pore size of 6.5–6.9 nm. The zeolite used in this study has a similar specific surface area and pore size compared to the same type of zeolite used in the literature [44,45]. Activated carbon is less charged with

zeta potential of −17.2 mV, comparing to −30.9 mV for zeolite. Our research plan involved using zeolite as a model sorbent to simulate the mineral geo-sorbents in soil; the chosen zeolite has similar porosity and physio-chemical properties to mineral soils.

At temperatures between 10 and 50 °C and electric field intensities between 0 and 3 V cm^{-1}, the degree and rate of PFOS adsorption were measured. The normalized effluent PFOS concentration C/C_0 was used to depict breakthrough curves (Figure 3). At all temperatures and electric field intensities, the C/C_0 ratio of zeolite (0.74–0.84) was significantly greater than that of activated carbon (0.35–0.60), resulting in a significantly higher PFOS concentration in the adsorbent after 48 h for activated carbon (15.6 ± 0.88–25.5 ± 1.01 mg g^{-1}) than for zeolite (0.26 ± 0.03–0.40 ± 0.04 mg g^{-1}). The rising temperature increased C/C_0 for both adsorbents, and heating increased the C/C_0 ratio of PFOS on activated carbon and zeolite by 50.3% and 9.7%, respectively, resulting in the PFOS concentration in the adsorbent at 48 h being reduced by 26.7% for activated carbon while there was a 18.8% reduction for zeolite. The electric field increased the PFOS adsorption on activated carbon (C/C_0 decreased up to 8.6%) and decreased the PFOS adsorption on zeolite (C/C_0 increased up to 5.5%), resulting in the PFOS concentration increased from 15.6 ± 0.88 to 18.7 ± 1.13 mg g^{-1} ($p < 0.05$) on activated carbon, while it decreased from 0.29 ± 0.03 to 0.26 ± 0.03 mg g^{-1} ($p < 0.05$) on zeolite. These findings are consistent with our previous research on electrokinetic effects on phenanthrene adsorption at room temperature [31].

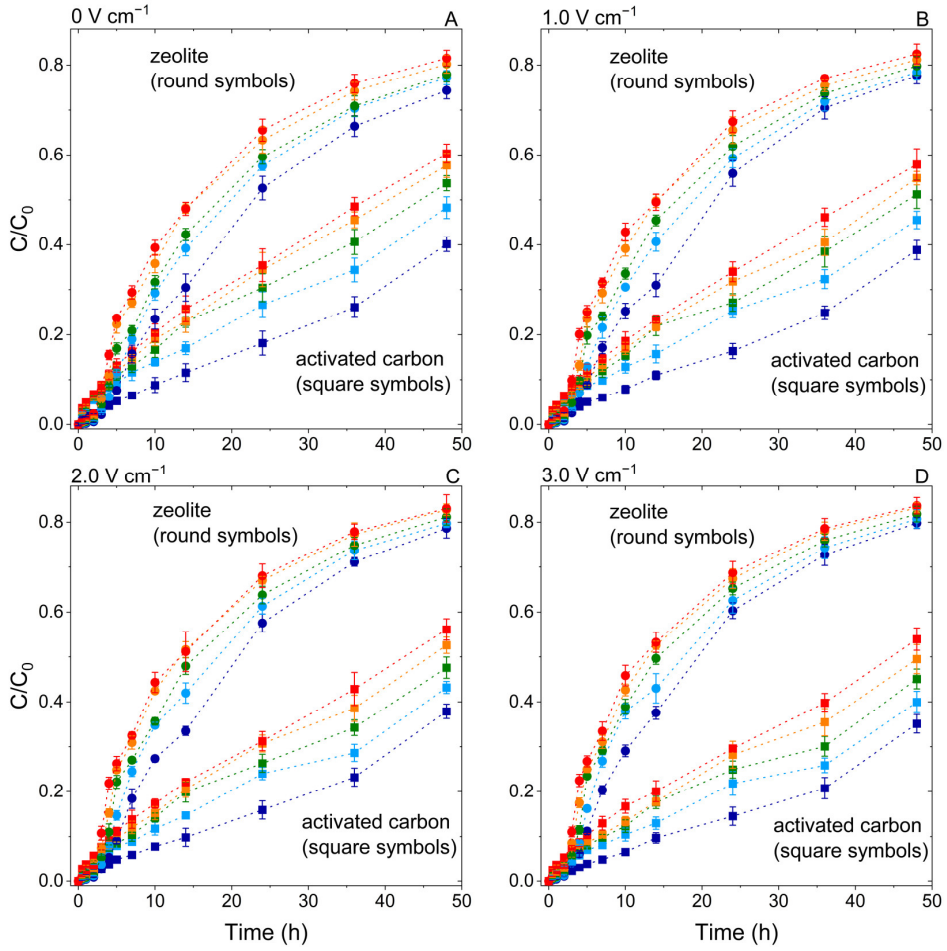

Figure 3. Normalized effluent PFOS concentration (C/C_0) over the adsorption time through the zeolite (round symbols) and activated carbon (square symbols) packed porous media, under 10 °C (dark blue lines), 20 °C (light blue lines), 30 °C (green lines), 40 °C (orange lines), and 50 °C (red lines), and DC fields 0 V cm^{-1} (**A**), 1 V cm^{-1} (**B**), 2 V cm^{-1} (**C**), and 3 V cm^{-1} (**D**).

Table 2. Basic properties of activated carbon and zeolite.

Adsorbent	Specific Surface Area	Pore Size	Zeta Potentia ζ
	(m^2 g^{-1})	(nm)	(mV)
Activated carbon	144.4	6.9	−17.2
Zeolite	2.9	6.5	−30.9

3.2. Temperature-Regulated PFOS Adsorption Kinetics and Thermodynamics

Pseudo-first-order and the pseudo-second-order were used to analyze the breakthrough curves: example of 0 V cm^{-1} and 3 V cm^{-1} conditions (Figure 4). The adsorption of PFOS was more consistent with the pseudo-second-order kinetic model due to the better regression correlations of the pseudo-second-order kinetic model with all $R^2 \geq 0.94$ (Tables 3 and 4). To quantify the adsorption kinetics, subsequent analyses used the kinetic constants of a pseudo-second-order kinetic model. Physically, the kinetic constants represent the rate of adsorption and indicate the amount of adsorbent required to adsorb 1 mg of adsorbate (PFOS) per unit time (per hour: h^{-1}). It should be noted that the value of k_2 decreased as adsorption rate increased [37].

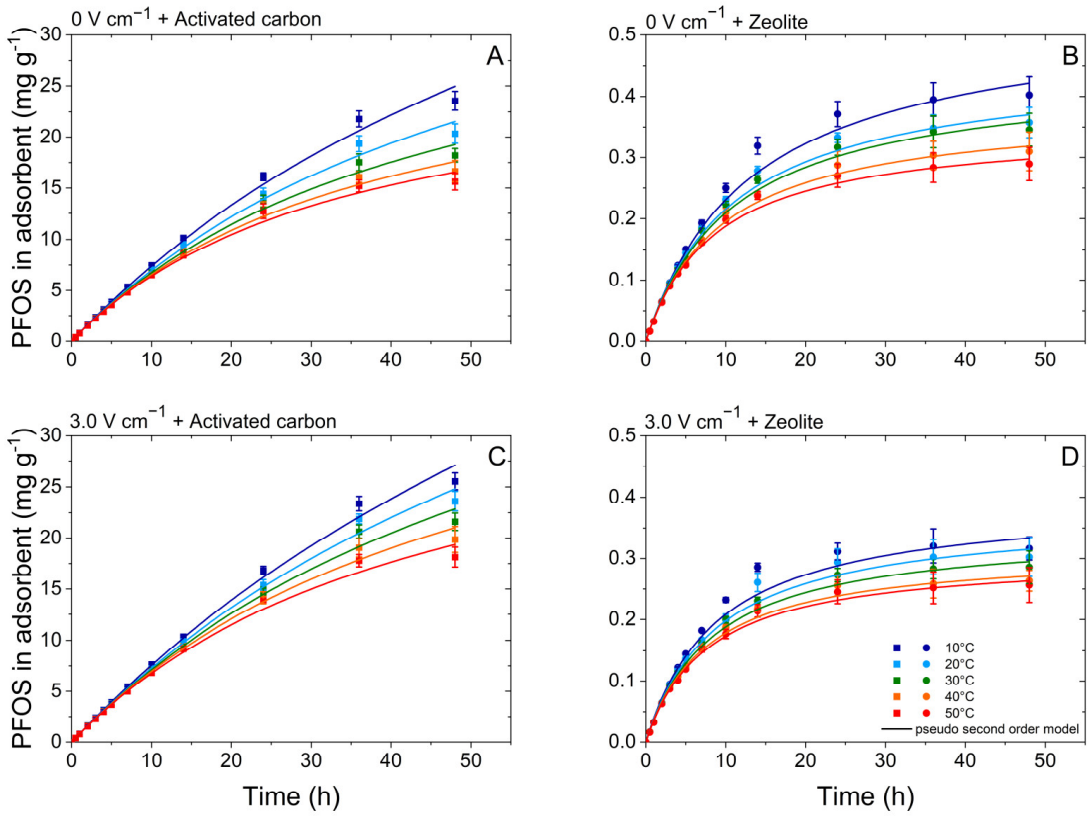

Figure 4. Temperature (10 to 50 °C) regulated PFOS adsorption kinetics on activated carbon (**A**,**C**) and zeolite (**B**,**D**) at electric field strengths 0 and 3 V cm^{-1}.

Table 3. Kinetic parameters of the pseudo-second-order model for PFOS adsorption on the two adsorbents at different temperatures and DC field strengths.

Adsorbent	Temperature °C	Pseudo-Second-Order Parameters with the Absence of DC Fields			Pseudo-Second-Order Parameters under 1 V cm^{-1}			Pseudo-Second-Order Parameters under 2 V cm^{-1}			Pseudo-Second-Order Parameters under 3 V cm^{-1}		
		q_e	k_2 (10^{-3})	R^2	q_e	k_2 (10^{-3})	R^2	q_e	k_2 (10^{-3})	R^2	q_e	k_2 (10^{-3})	R^2
Activated carbon	10	66.7	0.19	0.95	70.9	0.17	0.94	74.6	0.15	0.94	84.0	0.12	0.94
	20	47.9	0.36	0.97	52.9	0.29	0.97	59.5	0.23	0.96	67.6	0.18	0.96
	30	37.8	0.57	0.97	41.7	0.47	0.97	48.5	0.35	0.97	55.0	0.27	0.96
	40	31.6	0.83	0.98	36.2	0.63	0.97	39.5	0.53	0.97	44.8	0.42	0.97
	50	28.4	1.03	0.98	31.3	0.85	0.98	34.3	0.71	0.97	39.6	0.52	0.98
Zeolite	10	0.54	139.6	0.98	0.45	213.7	0.98	0.43	238.4	0.98	0.40	280.8	0.98
	20	0.46	195.8	0.99	0.43	228.9	0.99	0.39	280.4	0.99	0.37	302.1	0.99
	30	0.44	205.2	0.99	0.39	266.1	0.99	0.36	313.1	0.99	0.35	343.0	0.99
	40	0.38	273.7	1.00	0.36	311.1	1.00	0.32	390.5	1.00	0.31	421.4	1.00
	50	0.35	326.6	1.00	0.33	366.9	1.00	0.32	395.8	1.00	0.30	434.6	1.00

Table 4. Kinetic parameters of the pseudo-first-order model for PFOS adsorption on the two adsorbents at different temperatures and DC field strengths.

Adsorbent	Temperature °C	Pseudo-First-Order Parameters with the Absence of DC Fields			Pseudo-First-Order Parameters under 1 V cm^{-1}			Pseudo-First-Order Parameters under 2 V cm^{-1}			Pseudo-First-Order Parameters under 3 V cm^{-1}		
		q_e	k_1	R^2	q_e	k_1	R^2	q_e	k_1	R^2	q_e	k_1	R^2
Activated carbon	10	57.24	0.18	0.74	57.60	0.17	0.74	57.68	0.17	0.74	59.84	0.17	0.74
	20	47.10	0.17	0.77	50.11	0.17	0.75	50.80	0.17	0.77	54.10	0.17	0.75
	30	39.15	0.17	0.81	41.09	0.17	0.79	44.63	0.16	0.78	45.98	0.16	0.80
	40	34.14	0.17	0.82	35.37	0.16	0.88	37.68	0.16	0.84	40.17	0.16	0.81
	50	30.30	0.16	0.85	32.12	0.16	0.83	33.12	0.16	0.87	35.72	0.16	0.82
Zeolite	10	0.57	0.15	0.94	0.50	0.19	0.97	0.44	0.20	0.97	0.43	0.21	0.95
	20	0.49	0.15	0.92	0.46	0.16	0.92	0.43	0.16	0.90	0.41	0.19	0.90
	30	0.46	0.15	0.96	0.43	0.16	0.92	0.39	0.17	0.97	0.37	0.16	0.96
	40	0.40	0.15	0.93	0.39	0.15	0.92	0.33	0.15	0.96	0.32	0.16	0.95
	50	0.35	0.15	0.94	0.33	0.15	0.94	0.33	0.15	0.93	0.31	0.15	0.94

With the temperature increasing from 10 to 50 °C, the k_2 value increased at all DC electric field strengths. In the absence of DC fields, heating increased the adsorption kinetic constant of PFOS from 0.19 to 1.03 (ca. 442.1%) on activated carbon, and from 139.6 to 326.6 (ca. 134.0%) on zeolite. Similar trends were observed in the presence of DC fields, with rates of k_2 variation ranging from 10 to 50 °C on activated carbon of 400.0% at 1 V cm^{-1}, 373.3% at 2 V cm^{-1}, to 346.2% at 3 V cm^{-1}, and on zeolite of 71.6% at 1 V cm^{-1}, 66.0% at 2 V cm^{-1}, to 55.5% at 3 V cm^{-1}. Summarizing these results, it can be affirmed that the temperature–electrokinetically regulated adsorption was better than a single technique.

Temperature effects can be quantitatively described by the adsorption equilibrium properties, which may be depicted using isotherm and thermodynamic parameters. The isotherms represented the equilibrium adsorption properties at different temperatures. The Freundlich equation and Langmuir equation were used to analyze isotherm data. The regression correlations of the Langmuir model of PFOS adsorption on activated carbon ranged from 0.88 to 0.89 and from 0.98 to 0.99 on zeolite. In contrast, the regression correlations of the Freundlich equation were all higher than 0.97 (Table 5). As a result, the Freundlich equation was adopted to characterize the isotherms and calculate the thermodynamic parameters.

Table 5. Overview of the sorbents and their temperature-dependent Freundlich adsorption isotherm parameters (K_F and n) and Langmuir adsorption isotherm parameters (Q_{max} and K_L) of PFOS adsorption in 100 mmol L^{-1} electrolytes.

Adsorbent	Temperature	Freundlich Isotherm Parameters			Langmuir Isotherm Parameters		
	(°C)	*log* K_F	*n*	R^2	Q_{max} (mg g^{-1})	K_L (10^3 L mg^{-1})	R^2
Activated carbon	10	6.09	0.43	0.99	925.9	21.60	0.89
	20	6.03	0.42	0.98	909.1	18.33	0.89
	30	5.92	0.41	0.99	900.9	12.33	0.89
	40	5.88	0.42	0.97	885.0	9.42	0.88
	50	5.85	0.42	0.97	877.2	8.14	0.88
Zeolite	10	3.90	0.78	0.98	19.23	0.71	0.99
	20	3.86	0.77	0.98	18.52	0.64	0.98
	30	3.83	0.79	0.99	17.86	0.60	0.98
	40	3.77	0.81	0.99	15.87	0.54	0.99
	50	3.70	0.81	1.00	14.93	0.48	0.99

Thermodynamic parameters were used to further interpret temperature regulated PFOS adsorption. ΔG, ΔH and ΔS of PFOS adsorption were calculated (Table 6). Negative ΔG values (−24.7 to −47.0 kJ mol^{-1}) indicated spontaneous adsorption of PFOS on both adsorbents. Negative ΔH and positive ΔS showed an exothermic and entropy reduction process during PFOS adsorption. The adsorption strengths, represented by ΔG [31], ranged from −42.3 to −47.0 kJ mol^{-1} for activated carbon and from −24.7 to −26.5 kJ mol^{-1} for zeolite, between 10 and 50 °C.

Table 6. Overview of the thermodynamic parameters (ΔG, ΔH, and ΔS) of PFOS adsorption calculated based on Freundlich isotherm parameters.

Adsorbent	Temperature	ΔG	ΔH	ΔS
	(°C)	(kJ mol^{-1})	(kJ mol^{-1})	(kJ mol^{-1} k^{-1})
Activated carbon	10	−42.26 ± 0.34	−9.79 ± 1.44	0.12 ± 0.01
	20	−43.68 ± 0.34		
	30	−44.69 ± 0.11		
	40	−45.66 ± 0.24		
	50	−47.01 ± 1.18		
Zeolite	10	−24.70 ± 0.49	−12.92 ± 1.16	0.042 ± 0.003
	20	−25.48 ± 0.50		
	30	−25.90 ± 0.69		
	40	−26.03 ± 0.56		
	50	−26.51 ± 0.55		

3.3. Electrokinetic-Regulated PFOS Adsorption Kinetics

The effects of electrokinetic on adsorption kinetics at various temperatures were analyzed using the pseudo-second-order kinetic model, separately (Figure 5). The pseudo-second-order kinetic constant k_2 was adopted to quantitatively describe the electrokinetic regulated PFOS adsorption. With DC electric field strength increasing from 0 to 3 V cm^{-1}, the k_2 value decreased for activated carbon while increasing for zeolite for all temperatures: example of 10 °C and 50 °C conditions (Figure 5 and Table 4). Compared to using no DC electric field strength, a 3 V cm^{-1} electric field decreased k_2 from 0.19 to 0.12 (ca. 36.8%) on activated carbon, while increasing k_2 from 139.6 to 280.8 (ca. 101.1%) on zeolite at 10 °C. Similar electrokinetic effect trends were observed under temperatures ranging from 20 to 50 °C, with rates of variation on activated carbon ranging from 50%, 52.6%, 49.4%, to 49.5%, and from 54.3%, 67.2%, 54.0%, to 33.1% on zeolite.

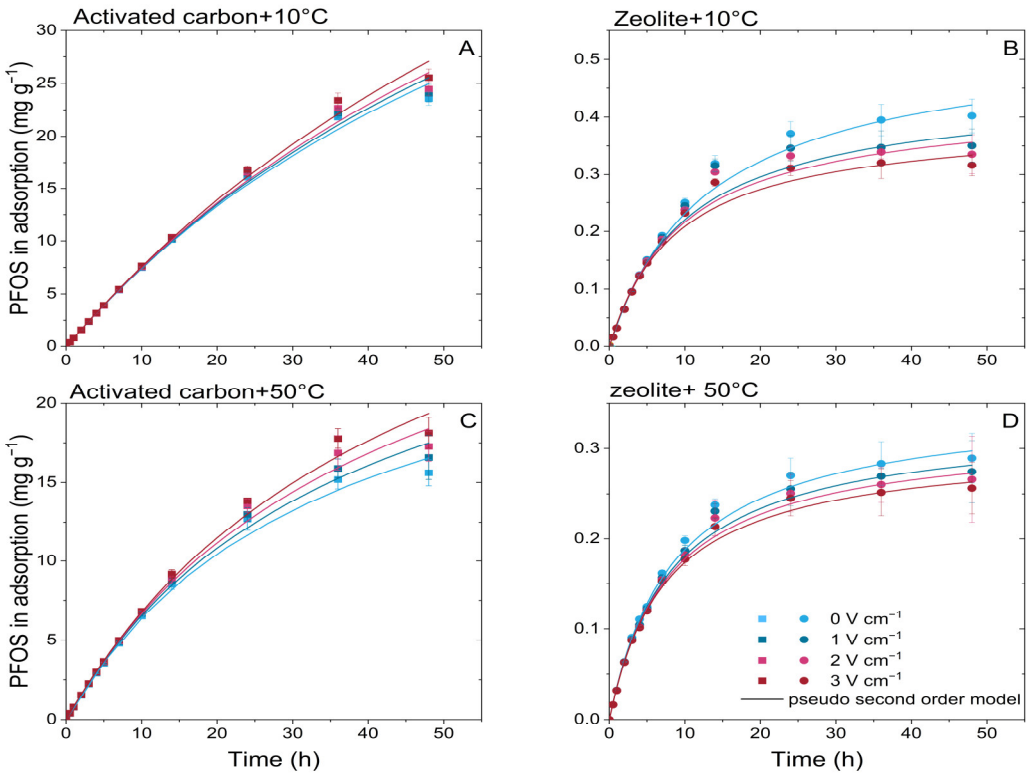

Figure 5. Electrokinetic regulated PFOS adsorption kinetics (at electric field strengths 0–3 V cm^{-1}) on activated carbon (**A**,**C**) and zeolite (**B**,**D**) under temperatures of 10 °C and 50 °C.

3.4. Temperature–Electrokinetic Regulated PFOS Adsorption

To further understand the temperature–electrokinetic co-driven mechanisms, the effects of temperature and electrokinetic on the variations of adsorption kinetic constants k_2 were depicted. (Figure 6). It is important to note that there are four steps associate with transport processes during adsorption by porous adsorbents. The first step is transport in the solution phase (known as "bulk transport"). The second step is "film diffusion". The third step involves diffusion of the adsorbate molecules from the exterior of the adsorbent into the pores of the adsorbent, along pore-wall surfaces, or both (known as "intraparticle diffusion") The last step is adsorptive attachment [28]. PFOS is homogeneously distributed in the bulk liquid, therefore, the bulk transport is not a limit step of its adsorption. While the electroosmotic flow controls the liquid flow of the film in an area adjacent to the sorbent surface, it is essential for film diffusion, which determines sorption kinetics. Therefore, we considered electroosmotic flow as the possible driving factor rather than electro-migration. It should be noted that the EOF velocity is co-driven by the effects of both electrokinetic and temperature, while at the same time the adsorption capacity varies with temperature. Temperature plays an essential role by varying the liquid viscosity, resulting in significant variations of EOF velocity. The k_2 values were found to be linearly correlated to the temperature–electrokinetic co-driven EOF velocity ($R^2 \geq 0.93$, $p < 0.01$) (Figure 6 and Table 7), the fitting slope values (Table 7) were found to be negatively related to the temperature, and the slope values differ due to temperature effects on the adsorption capacity. For activated carbon, the slopes of kinetic constant variation were negative, with the slopes decreasing with increasing temperature. While the slopes of kinetic constant variation were positive for zeolite, the slope values decreased with increasing temperature.

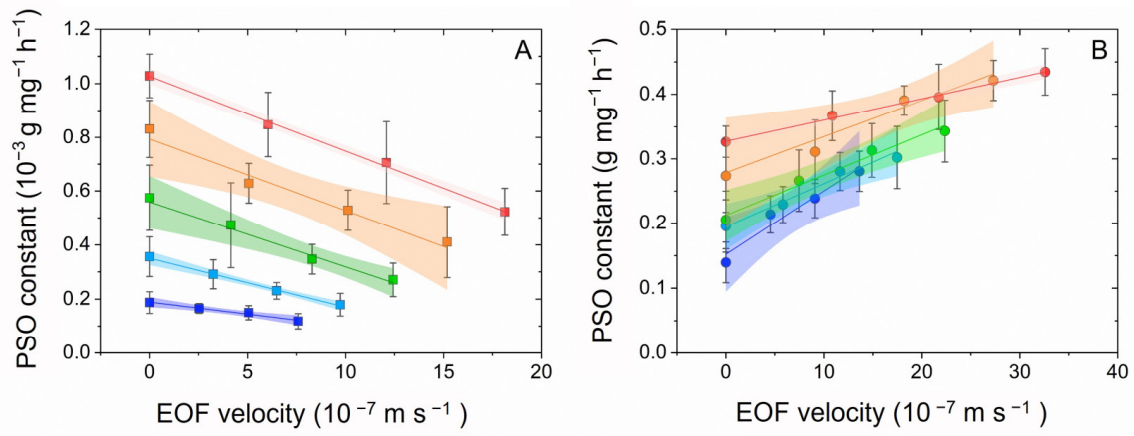

Figure 6. Temperature effects on the pseudo-second-order adsorption kinetic constant exposed to various electroosmotic flow velocities at temperature 10 °C (blue), 20 °C (light blue), 30 °C (green), 40 °C (orange), and 50 °C (red) on activated carbon (**A**) and zeolite (**B**).

Table 7. Linear fitting results of the slope and intercept values of pseudo-second-order kinetic constants and EOF velocities, with standard errors, *p* and R^2 values as quality control of static fitting.

	Intercept	Std. Error	*p*	Slope	Std. Error	*p*	R^2
AC−10 [a]	0.19	0.004	0.000	−0.009	0.001	0.009	0.98
AC−20	0.35	0.004	0.000	−0.018	0.001	0.001	1.00
AC−30	0.57	0.012	0.000	−0.025	0.002	0.004	0.98
AC−40	0.81	0.030	0.001	−0.027	0.003	0.013	0.96
AC−50	1.01	0.011	0.001	−0.027	0.001	0.003	1.00
ZE−10 [b]	0.15	0.013	0.007	0.010	0.002	0.023	0.95
ZE−20	0.20	0.007	0.001	0.006	0.001	0.011	0.97
ZE−30	0.21	0.009	0.002	0.006	0.001	0.011	0.98
ZE−40	0.27	0.012	0.002	0.006	0.001	0.015	0.97
ZE−50	0.33	0.029	0.000	0.003	0.000	0.002	1.00

[a] "AC" represents the activated carbon while "10" represents the temperature under 10 °C. [b] "ZE" represents the zeolite while "10" represents the temperature under 10 °C.

Based on the previously mentioned physical meanings of k_2, the slope values of kinetic constants vs. the EOF velocities correspond to the variation of PFOS adsorption rate caused per unit EOF velocity. Similarly, the slope values at different temperatures represent the temperature effects on EOF efficiencies. The EOF efficiencies on activated carbon decreased from −0.009 to −0.027 as the temperature increased from 10 to 50 °C. This indicated that the synergistic effect of temperature enhanced EOF efficiencies (the negative sign denotes EOF enhanced adsorption) is 3.0-fold for activated carbon. On the other hand, from 10 to 50 °C, the EOF efficiencies decreased from 0.01 to 0.003, indicating that the synergistic effect of temperature increased EOF efficiencies is 3.3-fold for zeolite (the positive slope values stand for EOF increased adsorption). It can be concluded that the temperature and electrokinetic synergy demonstrated much stronger regulating kinetics than single factors, the synergistic effects are controlled by the temperature–electrokinetic co-driven EOF velocity and temperature driven adsorption capacity.

3.5. Temperature–Electrokinetic Interactions and Their Regulation Framework

Furthermore, we investigated the temperature–electrokinetic co-driven PFOS adsorption from an energy standpoint by correlating ΔG, which could indicate the adsorption strength (thermodynamically), the electroosmotic flow velocity, showing the adsorption strength (kinetically), and the resultant kinetic constant variations (Figure 7). This extended previous established approaches from room temperature to a wider temperature range.

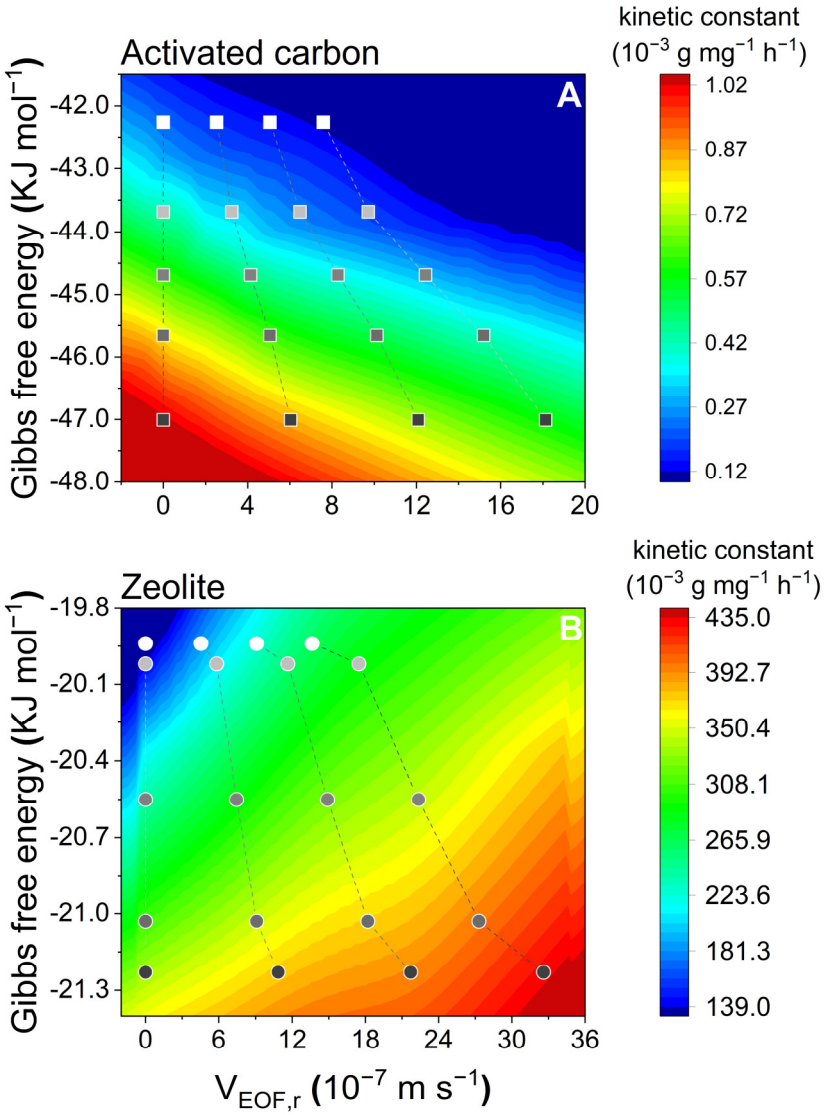

Figure 7. Interactions between electroosmotic flow velocities ($V_{EOF,r}$) and the Gibbs free energy (G), resulting in kinetic constant variations.

However, as the adsorption strength is derived thermodynamically, this approach has a problem in describing the mechanisms between thermodynamic parameters and kinetic parameters. Hence, based on the previous discussions, as an essential parameter of temperature, viscosity was chosen to interlink with EOF velocity and the kinetic constant k_2 to develop the approach to depict the mechanisms from a pure kinetic perspective (Figure 8). Higher liquid viscosity and higher EOF velocity generally result in enhanced adsorption (in the cold color areas in Figure 8A). In contrast, smaller liquid viscosity and a higher EOF velocity appear to result in electrokinetic suppression of PFOS adsorption (warm color areas in Figure 8B). The established approach, thus, can depict the temperature–electrokinetic co-driven PFOS adsorption kinetics.

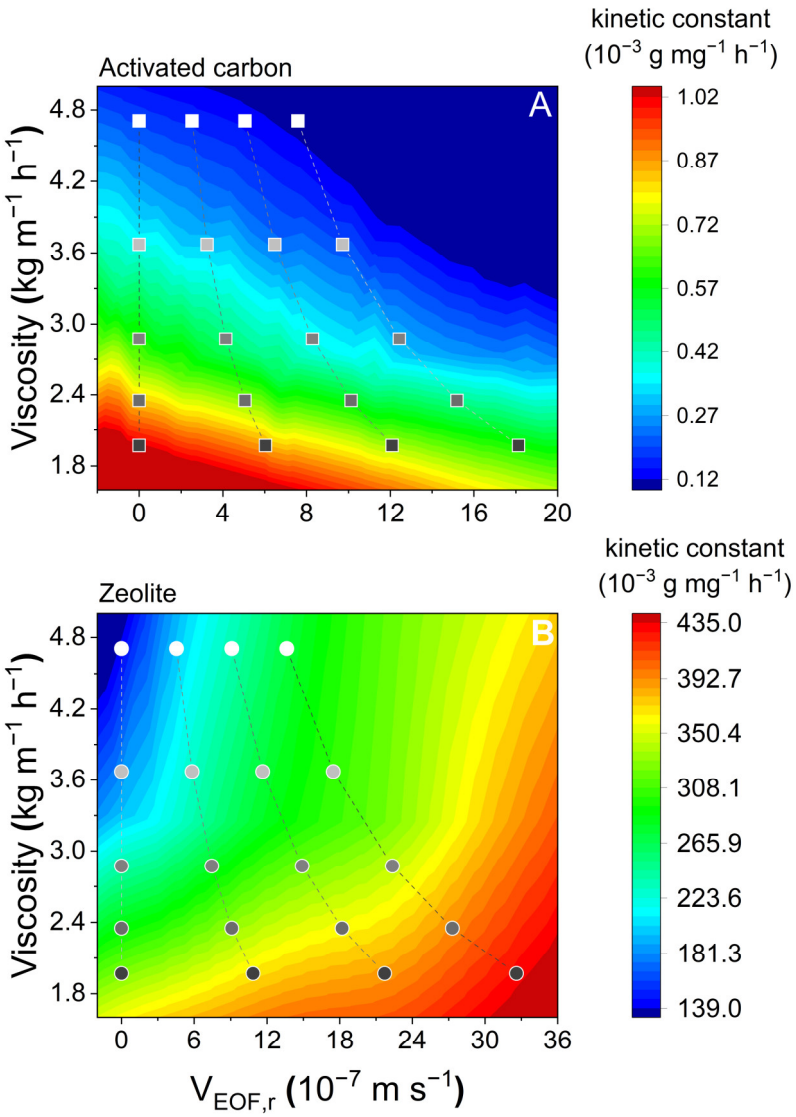

Figure 8. Interactions between electroosmotic flow velocities ($V_{EOF,r}$) and the viscosity (η) resulted from kinetic constant variations.

3.6. Potential Engineering Applications

The transport of contaminants is the main threat to ecosystems and humans. For example, the low adsorption capacity or high permeability of soil porous media may impose severe limitations on bioconversion rates while threatening groundwater security [46–48]. To ensure the safety of drinking water, environmental biotechnology must manage and control contaminants transport [49]. Annual temperature fluctuations may surpass 40 °C in regions with strong seasonal temperature swings, which would be an obvious factor. Using adsorbents which were either purely mineral or carbonaceous, we argued that temperature, in conjunction with EOF, might be utilized to regulate PFOS-matrix interactions as a driver for determining the fate of PFOS and protecting drinking water safety. Moreover, the effect of electroosmotic flow is proportional to the intensity of the electric field, which can be amplified in practice to produce larger effects. Because soil matrices in natural systems frequently contain a mixture of mineral and carbonaceous elements, it is challenging to anticipate the effects of temperature and electrokinetics on adsorption processes. It is essential to elucidate the soil composition, physio-chemical properties, adsorption thermodynamic parameters, and the kinetic properties to forecast the impacts of temperature on electrokinetically regulated PFOS-matrix interactions.

On the other hand, for the treatment of PFOS-contaminated groundwater, low temperature coupling electrokinetics on carbonaceous adsorbents may increase the adsorption capacity, reducing the waste adsorption materials and preventing the risk of PFOS emission. In environmental (bio-)technology, temperature and electrokinetic methods may be used to fine-tune the kinetics of the interaction between adsorbates and adsorbents. This kinetic regulation may lead to future technical applications that restrict adsorption processes, such as in response to fluctuating adsorbate concentrations in contaminated water streams, in electro-bioremediation, or to prevent unwanted adsorption of solutes in technical applications.

4. Conclusions

We investigated the temperature–electrokinetic adsorption mechanisms of PFOS on porous column media packed with two typical geo-adsorbents, activated carbon and zeolite. DC fields increased PFOS adsorption on activated carbon while decreasing it on zeolite. Increasing temperature decreased PFOS adsorption on both adsorbents also in the presence of DC fields. The DC electric field effect was found to be correlated with the rate of electroosmotic flow. The temperature changed the DC field effect by changing the viscosity of the liquid. Then, an approach correlating viscosity-EOF velocity-adsorption kinetics was developed, predicting the adsorption of PFOS regulated by temperature and electrokinetics. This kinetic approach may predict temperature–electrokinetic co-driven PFOS adsorption in various natural and man-made porous media in technical applications.

Author Contributions: Conceptualization, Y.Y., Y.S., D.M., L.Y. (Liuqing Yang), M.Z., W.J. and L.Y. (Lichu Yin); methodology, Y.Y., Y.S., D.M., P.L., B.L., W.J. and L.Y. (Lichu Yin); validation, Y.Y.; formal analysis, Y.Y. and Y.S.; investigation, Y.Y.; data curation, Y.Y. and Y.S.; writing—original draft, Y.Y.; writing—review & editing, Y.Y., Y.S., B.Z. and W.J.; supervision, W.J.; funding acquisition, Y.S. and W.J. All authors have read and agreed to the published version of the manuscript.

Funding: The National Natural Science Foundation of China (Grant No. 42277011), and the fellowship of the China Postdoctoral Science Foundation (2022M713300).

Data Availability Statement: Not applicable.

Conflicts of Interest: The authors declare no conflict of interest. The funders had no role in the design of the study; in the collection, analyses, or interpretation of data; in the writing of the manuscript; or in the decision to publish the results.

References

1. Evich, M.G.; Davis, M.J.B.; McCord, J.P.; Acrey, B.; Awkerman, J.A.; Knappe, D.R.U.; Lindstrom, A.B.; Speth, T.F.; Tebes-Stevens, C.; Strynar, M.J.; et al. Per- and polyfluoroalkyl substances in the environment. *Science* **2022**, *375*, eabg9065. [CrossRef] [PubMed]
2. Grandjean, P.; Heilmann, C.; Weihe, P.; Nielsen, F.; Mogensen, U.B.; Budtz-Jørgensen, E. Serum Vaccine Antibody Concentrations in Adolescents Exposed to Perfluorinated Compounds. *Environ. Health Perspect.* **2017**, *125*, 077018. [CrossRef] [PubMed]
3. Gar Alalm, M.; Boffito, D.C. Mechanisms and pathways of PFAS degradation by advanced oxidation and reduction processes: A critical review. *Chem. Eng. J.* **2022**, *450*, 138352. [CrossRef]
4. Sunderland, E.M.; Hu, X.C.; Dassuncao, C.; Tokranov, A.K.; Wagner, C.C.; Allen, J.G. A review of the pathways of human exposure to poly- and perfluoroalkyl substances (PFASs) and present understanding of health effects. *J. Expo. Sci. Environ. Epidemiol.* **2019**, *29*, 131–147. [CrossRef]
5. Li, Y.; Barregard, L.; Xu, Y.; Scott, K.; Pineda, D.; Lindh, C.H.; Jakobsson, K.; Fletcher, T. Associations between perfluoroalkyl substances and serum lipids in a Swedish adult population with contaminated drinking water. *Environ. Health* **2020**, *19*, 33. [CrossRef]
6. Mastrantonio, M.; Bai, E.; Uccelli, R.; Cordiano, V.; Screpanti, A.; Crosignani, P. Drinking water contamination from perfluoroalkyl substances (PFAS): An ecological mortality study in the Veneto Region, Italy. *Eur. J. Public Health* **2018**, *28*, 180–185. [CrossRef]
7. Stanifer, J.W.; Stapleton, H.M.; Souma, T.; Wittmer, A.; Zhao, X.; Boulware, L.E. Perfluorinated Chemicals as Emerging Environmental Threats to Kidney Health. *Clin. J. Am. Soc. Nephrol.* **2018**, *13*, 1479. [CrossRef]
8. Podder, A.; Sadmani, A.H.M.A.; Reinhart, D.; Chang, N.-B.; Goel, R. Per and poly-fluoroalkyl substances (PFAS) as a contaminant of emerging concern in surface water: A transboundary review of their occurrences and toxicity effects. *J. Hazard. Mater.* **2021**, *419*, 126361. [CrossRef]

9. Batzella, E.; Girardi, P.; Russo, F.; Pitter, G.; Da Re, F.; Fletcher, T.; Canova, C. Perfluoroalkyl substance mixtures and cardiometabolic outcomes in highly exposed male workers in the Veneto Region: A mixture-based approach. *Environ. Res.* **2022**, *212*, 113225. [CrossRef]
10. Crone, B.C.; Speth, T.F.; Wahman, D.G.; Smith, S.J.; Abulikemu, G.; Kleiner, E.J.; Pressman, J.G. Occurrence of Per- and Polyfluoroalkyl Substances (PFAS) in Source Water and Their Treatment in Drinking Water. *Crit. Rev. Environ. Sci. Technol.* **2019**, *49*, 2359–2396. [CrossRef]
11. Tukker, A.M.; Bouwman, L.M.S.; van Kleef, R.G.D.M.; Hendriks, H.S.; Legler, J.; Westerink, R.H.S. Perfluorooctane sulfonate (PFOS) and perfluorooctanoate (PFOA) acutely affect human $\alpha 1\beta 2\gamma 2$L GABAA receptor and spontaneous neuronal network function in vitro. *Sci. Rep.* **2020**, *10*, 5311. [CrossRef]
12. Svensson, K.; Tanner, E.; Gennings, C.; Lindh, C.; Kiviranta, H.; Wikström, S.; Bornehag, C.-G. Prenatal exposures to mixtures of endocrine disrupting chemicals and children's weight trajectory up to age 5.5 in the SELMA study. *Sci. Rep.* **2021**, *11*, 11036. [CrossRef]
13. Hou, J.; Li, G.; Liu, M.; Chen, L.; Yao, Y.; Fallgren, P.H.; Jin, S. Electrochemical destruction and mobilization of perfluorooctanoic acid (PFOA) and perfluorooctane sulfonate (PFOS) in saturated soil. *Chemosphere* **2022**, *287*, 132205. [CrossRef]
14. Amii, H.; Uneyama, K. C–F bond activation in organic synthesis. *Chem. Rev.* **2009**, *109*, 2119–2183. [CrossRef]
15. Sharma, S.; Shetti, N.P.; Basu, S.; Nadagouda, M.N.; Aminabhavi, T.M. Remediation of per- and polyfluoroalkyls (PFAS) via electrochemical methods. *Chem. Eng. J.* **2022**, *430*, 132895. [CrossRef]
16. Dixit, F.; Dutta, R.; Barbeau, B.; Berube, P.; Mohseni, M. PFAS removal by ion exchange resins: A review. *Chemosphere* **2021**, *272*, 129777. [CrossRef]
17. Li, Y.; Liang, Y.-Q.; Mao, X.-M.; Li, H. Efficient removal of Cu(II) from an aqueous solution using a novel chitosan assisted EDTA-intercalated hydrotalcite-like compound composite: Preparation, characterization, and adsorption mechanism. *Chem. Eng. J.* **2022**, *438*, 135531. [CrossRef]
18. Loganathan, N.; Wilson, A.K. Adsorption, Structure, and Dynamics of Short- and Long-Chain PFAS Molecules in Kaolinite: Molecular-Level Insights. *Environ. Sci. Technol.* **2022**, *56*, 8043–8052. [CrossRef]
19. Shakya, A.; Vithanage, M.; Agarwal, T. Influence of pyrolysis temperature on biochar properties and Cr(VI) adsorption from water with groundnut shell biochars: Mechanistic approach. *Environ. Res.* **2022**, *215*, 114243. [CrossRef]
20. Cui, J.; Gao, P.; Deng, Y. Destruction of Per- and Polyfluoroalkyl Substances (PFAS) with Advanced Reduction Processes (ARPs): A Critical Review. *Environ. Sci. Technol.* **2020**, *54*, 3752–3766. [CrossRef]
21. Gagliano, E.; Sgroi, M.; Falciglia, P.P.; Vagliasindi, F.G.A.; Roccaro, P. Removal of poly- and perfluoroalkyl substances (PFAS) from water by adsorption: Role of PFAS chain length, effect of organic matter and challenges in adsorbent regeneration. *Water Res.* **2020**, *171*, 115381. [CrossRef] [PubMed]
22. Meng, P.; Fang, X.; Maimaiti, A.; Yu, G.; Deng, S. Efficient removal of perfluorinated compounds from water using a regenerable magnetic activated carbon. *Chemosphere* **2019**, *224*, 187–194. [CrossRef] [PubMed]
23. Huang, J.; Shi, Y.; Huang, G.-z.; Huang, S.; Zheng, J.; Xu, J.; Zhu, F.; Ouyang, G. Facile Synthesis of a Fluorinated-Squaramide Covalent Organic Framework for the Highly Efficient and Broad-Spectrum Removal of Per- and Polyfluoroalkyl Pollutants. *Angew. Chem. Int. Ed.* **2022**, *61*, e202206749.
24. Ten Hulscher, T.E.M.; Cornelissen, G. Effect of temperature on sorption equilibrium and sorption kinetics of organic micropollutants—A review. *Chemosphere* **1996**, *32*, 609–626. [CrossRef]
25. Loganathan, P.; Vigneswaran, S.; Kandasamy, J.; Naidu, R. Defluoridation of drinking water using adsorption processes. *J. Hazard. Mater.* **2013**, *248–249*, 1–19. [CrossRef]
26. Qin, J.; Moustafa, A.; Harms, H.; El-Din, M.G.; Wick, L.Y. The power of power: Electrokinetic control of PAH interactions with exfoliated graphite. *J. Hazard. Mater.* **2015**, *288*, 25–33. [CrossRef]
27. Podolsky, R.D. Temperature and water viscosity: Physiological versus mechanical effects on suspension feeding. *Science* **1994**, *265*, 100–103. [CrossRef]
28. Tran, H.N.; You, S.-J.; Hosseini-Bandegharaei, A.; Chao, H.-P. Mistakes and inconsistencies regarding adsorption of contaminants from aqueous solutions: A critical review. *Water Res.* **2017**, *120*, 88–116. [CrossRef]
29. Sprocati, R.; Gallo, A.; Sethi, R.; Rolle, M. Electrokinetic Delivery of Reactants: Pore Water Chemistry Controls Transport, Mixing, and Degradation. *Environ. Sci. Technol.* **2021**, *55*, 719–729. [CrossRef]
30. Sprocati, R.; Rolle, M. On the interplay between electromigration and electroosmosis during electrokinetic transport in heterogeneous porous media. *Water Res.* **2022**, *213*, 118161. [CrossRef]
31. Shan, Y.; Qin, J.; Harms, H.; Wick, L.Y. Electrokinetic effects on the interaction of phenanthrene with geo-sorbents. *Chemosphere* **2020**, *242*, 125161. [CrossRef]
32. Sautel, M.; Elmaleh, H.; Leveiller, F. Comparison of Specific Surface Areas of a Micronized Drug Substance as Determined by Different Techniques. In *Studies in Surface Science and Catalysis*; Unger, K.K., Kreysa, G., Baselt, J.P., Eds.; Elsevier: Amsterdam, The Netherlands, 2000; pp. 633–642.
33. Nandi, D.; Shivrayan, M.; Gao, J.; Krishna, J.; Das, R.; Liu, B.; Thayumanavan, S.; Kulkarni, A. Core Hydrophobicity of Supramolecular Nanoparticles Induces NLRP3 Inflammasome Activation. *ACS Appl. Mater. Interfaces* **2021**, *13*, 45300–45314. [CrossRef]

34. Martin, J.; Gracia, A.R.; Asuero, A.G. Fitting Nonlinear Calibration Curves: No Models Perfect. *J. Anal. Sci. Methods Instrum.* **2017**, *7*, 74544. [CrossRef]
35. Askeland, M.; Clarke, B.O.; Cheema, S.A.; Mendez, A.; Gasco, G.; Paz-Ferreiro, J. Biochar sorption of PFOS, PFOA, PFHxS and PFHxA in two soils with contrasting texture. *Chemosphere* **2020**, *249*, 126072. [CrossRef]
36. Nguyen, T.M.H.; Braunig, J.; Thompson, K.; Thompson, J.; Kabiri, S.; Navarro, D.A.; Kookana, R.S.; Grimison, C.; Barnes, C.M.; Higgins, C.P.; et al. Influences of Chemical Properties, Soil Properties, and Solution pH on Soil-Water Partitioning Coefficients of Per- and Polyfluoroalkyl Substances (PFASs). *Environ. Sci. Technol.* **2020**, *54*, 15883–15892. [CrossRef]
37. Kopinke, F.-D.; Georgi, A.; Goss, K.-U. Comment on "Mistakes and inconsistencies regarding adsorption of contaminants from aqueous solution: A critical review, published by Tran et al. [Water Research 120, 2017, 88–116]". *Water Res.* **2018**, *129*, 520–521. [CrossRef]
38. Du, Z.; Deng, S.; Liu, D.; Yao, X.; Wang, Y.; Lu, X.; Wang, B.; Huang, J.; Wang, Y.; Xing, B.; et al. Efficient adsorption of PFOS and F53B from chrome plating wastewater and their subsequent degradation in the regeneration process. *Chem. Eng. J.* **2016**, *290*, 405–413. [CrossRef]
39. Li, X.; Wang, C.; Zhang, J.; Liu, J.; Liu, B.; Chen, G. Preparation and application of magnetic biochar in water treatment: A critical review. *Sci. Total Environ.* **2020**, *711*, 134847. [CrossRef] [PubMed]
40. Mangla, D.; Sharma, A.; Ikram, S. Critical review on adsorptive removal of antibiotics: Present situation, challenges and future perspective. *J. Hazard. Mater.* **2022**, *425*, 127946. [CrossRef] [PubMed]
41. Vallano, P.T.; Remcho, V.T. Modeling interparticle and intraparticle (perfusive) electroosmotic flow in capillary electrochromatography. *Anal. Chem.* **2000**, *72*, 4255–4265. [CrossRef]
42. Olivares, W.; Croxton, T.L.; McQuarrie, D.A. Electrokinetic flow in a narrow cylindrical capillary. *J. Phys. Chem.* **1980**, *84*, 867–869. [CrossRef]
43. Sharma, P.K.; Hanumantha Rao, K. Adhesion of Paenibacillus polymyxa on chalcopyrite and pyrite: Surface thermodynamics and extended DLVO theory. *Colloids Surf. B Biointerfaces* **2003**, *29*, 21–38. [CrossRef]
44. Abdullah, A.H.; Mat, R.; Somderam, S.; Abd Aziz, A.S.; Mohamed, A. Hydrogen sulfide adsorption by zinc oxide-impregnated zeolite (synthesized from Malaysian kaolin) for biogas desulfurization. *J. Ind. Eng. Chem.* **2018**, *65*, 334–342. [CrossRef]
45. de Aquino, T.F.; Estevam, S.T.; Viola, V.O.; Marques, C.R.M.; Zancan, F.L.; Vasconcelos, L.B.; Riella, H.G.; Pires, M.J.R.; Morales-Ospino, R.; Torres, A.E.B.; et al. CO_2 adsorption capacity of zeolites synthesized from coal fly ashes. *Fuel* **2020**, *276*, 118143. [CrossRef]
46. Baduel, C.; Mueller, J.F.; Rotander, A.; Corfield, J.; Gomez-Ramos, M.-J. Discovery of novel per- and polyfluoroalkyl substances (PFASs) at a fire fighting training ground and preliminary investigation of their fate and mobility. *Chemosphere* **2017**, *185*, 1030–1038. [CrossRef]
47. Weber, A.K.; Barber, L.B.; LeBlanc, D.R.; Sunderland, E.M.; Vecitis, C.D. Geochemical and hydrologic factors controlling subsurface transport of poly- and perfluoroalkyl substances, cape cod, massachusetts. *Environ. Sci. Technol.* **2017**, *51*, 4269–4279. [CrossRef]
48. Høisæter, Å.; Pfaff, A.; Breedveld, G.D. Leaching and transport of PFAS from aqueous film-forming foam (AFFF) in the unsaturated soil at a firefighting training facility under cold climatic conditions. *J. Contam. Hydrol.* **2019**, *222*, 112–122. [CrossRef]
49. Shojaei, M.; Kumar, N.; Chaobol, S.; Wu, K.; Crimi, M.; Guelfo, J. Enhanced Recovery of Per- and Polyfluoroalkyl Substances (PFASs) from Impacted Soils Using Heat Activated Persulfate. *Environ. Sci. Technol.* **2021**, *55*, 9805–9816. [CrossRef]